Tunable magnetic topological insulating phases in monolayer CrI_3

Santu Baidya,[1,2,*] Jaejun Yu,[3,†] and Choong H. Kim[1,2,‡]

[1]*Center for Correlated Electron Systems, Institute for Basic Science (IBS), Seoul 08826, Republic of Korea*

[2]*Department of Physics and Astronomy, Seoul National University, Seoul 08826, Republic of Korea*

[3]*Center for Theoretical Physics, Department of Physics and Astronomy, Seoul National University, Seoul 08826, Republic of Korea*

(Received 14 August 2018; published 30 October 2018)

We present results indicating that Chern insulator states can be achieved in the recently synthesized pristine chromium triiodide (CrI_3) by either electron or hole doping. Our first-principles density-functional-theory calculations confirmed that monolayer CrI_3 show nontrivial Chern number C in both the valence and conduction bands. By introducing on-site Coulomb interaction or epitaxial strain, the doped CrI_3 exhibit a series of topological quantum phase transitions between multiple Chern insulator phases as well as semimetal-to-insulator transitions. We show that the covalency of Cr d-I p bands controlled by the on-site Coulomb interaction U and strain is one of the key ingredients determining the topological phase and semimetal-insulator phase boundary.

DOI: 10.1103/PhysRevB.98.155148

I. INTRODUCTION

Over the past decade, magnetic topological insulators have attracted much attention from researchers due to their potential applications to low-energy consumption electronics and spintronics devices [1–3]. Chern insulators (CIs) with nonzero Chern number C [4,5], under broken time-reversal symmetry provide quantized anomalous Hall transport without an applied magnetic field and carry C dissipationless chiral edge states at the boundary [6]. There have been several attempts to realize CI states in real materials. The first successful attempt was made by doping chromium (Cr) or vanadium (V) into bismuth (Bi) or antimony $(Sb)_2Te_3$ thin film [7], but this required extreme conditions such as ultralow temperature. Since the magnetic atoms that induce magnetization in topological insulators initially exhibit time-reversal symmetry [8,9], the size of the induced magnetic splitting is limited by the exchange coupling of the magnetic dopants. Strong spin-orbit coupling (SOC) and magnetic instability are two key ingredients to stabilize a large gap CI. But they are in trade of relation since an element with strong SOC usually tends to be magnetically inactive. In such cases, the choice of the practically possible ratio between those degrees of freedoms puts a challenge in choosing correct transition-metal atoms.

Significant studies have been carried out to reconfigure and manipulate the boundary state in magnetic topological insulators to improve spintronics [7,10–12]. The chirality of the edge states in $(Bi_{1-y}Sb_y)_2Te_3$ magnetic TI thin film was controlled by the magnetization direction [10]. Even the position of the chiral edge states can be manipulated via domain control by either local magnetic field or current-induced spin-orbit torque [13,14]. Thus it would be interesting to show the tunability of chiral edge states in CIs and understand the physics behind this.

Recently, there has been increasing interest and new developments related to the so-called two-dimensional (2D) van-der-Waals materials [15]. It was theoretically suggested that topologically nontrivial phases may be realized in a monolayer of La (Lu) deposited on single-layer $CrSiTe_3$ ($CrGeTe_3$) even without spin-orbit coupling [16]. And ferromagnetic trihalide monolayers MnX_3 [17] and VX_3 [18] were proposed to be Dirac half-metals. But it is not yet verified experimentally if any monolayer trihalide would maintain Ising ferromagnetic ordering down to monolayer limit. All these previous works led us to look into new interesting 2D van-der-Waals material, chromium triiodide (CrI_3) reported to be an insulating ferromagnet with a Curie temperature (T_c) of 61 K, and is suggested to be a promising material for spintronic and magnetoelectronic research [19]. A recent measurement based on magneto-optic-Kerr-effect microscopy demonstrated that monolayered CrI_3 is an Ising ferromagnet with an out-of-plane spin orientation with $T_c = 45$ K, slightly lower than its bulk T_c. Since the strength of SOC for the I p orbitals is known as about 0.63 eV [20], this system may be a suitable candidate for a CI with a wide band gap.

In this paper, we demonstrate that CI phase can indeed be achieved in charge-doped monolayer CrI_3. From first-principles density-functional theory, the calculated Chern numbers confirm the existence of nontrivial band topologies in both the valence and conduction bands of the pristine monolayer CrI_3. Motivated by recent experiments on electrostatic gating on this compound [21,22], we suggest that the electron- or hole-doped CrI_3 would provide the CI phase. Unlike the other proposed systems, the nontrivial topology in the monolayer CrI_3 relies on the strong SOC of the coordinating I atoms. Even though Cr atoms, which are the main source of ferromagnetic instability, have very small atomic SOC strength, the strong SOC of I p states induces a rather large gap CI with the help of strong hybridization between Cr d and I p states near the Fermi level. Further, by the epitaxial

*santub@snu.ac.kr
†jyu@snu.ac.kr
‡chkim82@snu.ac.kr

strain or the Coulomb interaction U tuning, we can control the localizability of the Cr d state to induce a series of TQPTs, as well as a semimetal-to-insulator transition. Changes of chirality through TQPTs are clearly reflected in our edge state calculations to suggest the tunability of chiral edge states.

II. COMPUTATIONAL DETAILS

We carried out first-principles calculations based on density-functional theory (DFT) within the framework of the PBE-type generalized gradient approximation functional (PBE) [23] with on-site Coulomb interaction U for the Cr d orbitals, as implemented in the VASP package [24,25]. All of the calculations were performed with a plane-wave cutoff of 600 eV on the $8 \times 8 \times 1$ Γ-centered Monkhorst-Pack k-point mesh grid. The vacuum layer was set to be 20 Å thick to decouple neighboring layers along the z direction. The full relaxation was carried out by maintaining the threefold rotational symmetry and inversion symmetry inherent in the space group $R\bar{3}$ with forces smaller than 0.01 eV/Å. We also employed the OPENMX code [26] to conduct the symmetry analysis of the band structures and plot the molecular orbitals. The energy cutoff for OPENMX was set to 400 Ryd.

III. RESULTS

Figure 1(a) shows the crystal structure of pristine monolayer CrI_3. The fully relaxed optimized structure, as obtained from DFT calculations, exhibits a small trigonal distortion of the CrI_6 octahedron, but still preserves the space-group symmetry of $R\bar{3}$ with an optimized lattice constant of $a = 7.006$ Å, where the edge-shared CrI_6 octahedra form a honeycomb lattice of Cr atoms. Figures 1(c) and 1(d) show the band structures of monolayer CrI_3 near E_F with and without SOC, respectively. According to the DFT calculations based on the Perdew-Burke-Ernzerhof (PBE) exchange-correlation functional the ground state of monolayer CrI_3 was determined to be a ferromagnetic (FM) insulator with a band gap of about 1.2 eV without SOC and slightly less than 1.0 eV with SOC. From the comparison of the bands with and without SOC, one can easily conclude that the presence of strong SOC in the I p orbitals reduces the band gap with SOC by about 0.25 eV. Hence, we expect that the valence bands will broaden due to the strong hybridization of the Cr d-I p orbitals.

As illustrated in Fig. 1(b), the projected density of states (pDOS) for Cr and I atoms without SOC shows that a band gap is formed between the valence band maximum (VBM) of the Cr t_{2g}-I p hybridized states and the conduction band minimum (CBM) of the Cr e_g-I p hybridized states. The separation of Cr t_{2g} and e_g is about 1.7 eV, which we attributed to the ligand field splitting arising from the CrI_6 octahedron. The fully occupied Cr t_{2g} orbital states, located at about 0.5 eV below E_F, were identified as a source of magnetism corresponding to Cr^{3+} d^3 ($t_{2g}^{3\uparrow}$). The value calculated for the magnetic moment of $\sim 3.1\mu_B$ with a strong out-of-plane easy-axis anisotropy of $\sim$0.65 meV for the monolayer CrI_3 is also consistent with that reported in previous studies [19,27,28].

In addition to its FM insulator ground state [29,30], monolayer CrI_3 exhibits intriguing nontrivial topology in its

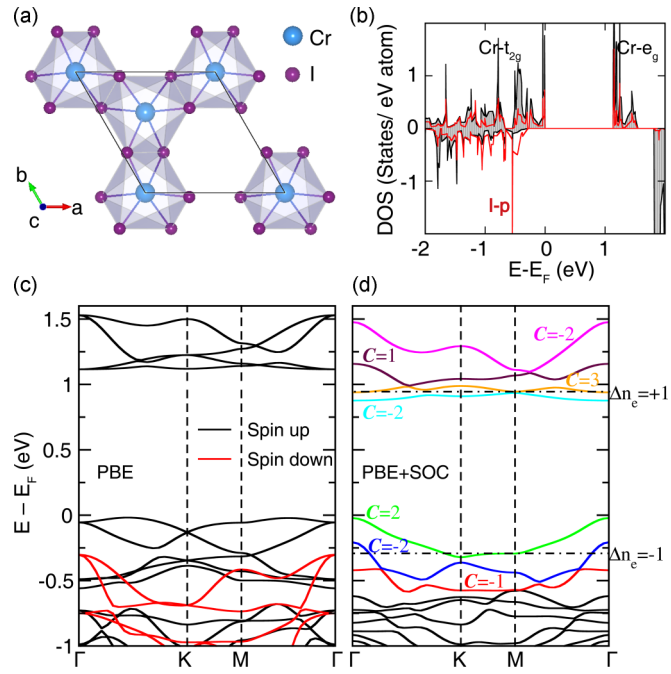

FIG. 1. (a) The crystal structure of pristine monolayer chromium triiodide (CrI_3) without doping. (b) The partial density of states of chromium (Cr)-d states and I-p states. The energy manifolds of the Cr-t_{2g} and e_g states are marked in the figure. (c) The Perdew-Burke-Ernzerhof (PBE) band structure. (d) The PBE+spin orbit coupling (SOC) band structure with Chern number C of each individual band within the energy manifold around the Fermi level is marked according to band color. The two dash-dotted lines labeled by $\Delta n_e = +1$ and $\Delta n_e = -1$ represent two Fermi levels for one electron and hole doping per $(CrI_3)_2$-unit cell, respectively.

conduction and valence bands. The nontrivial aspects of the conduction and valence bands are clearly manifested in the bands without SOC, as shown in Fig. 1(c). The conduction bands consist primarily of Cr e_g orbitals hybridized with I p states and form an e_g-manifold band structure. The conduction bands in Fig. 1(c) exhibit multiple crossings along the symmetry lines, which correspond to the multiple Dirac cones of the e_g bands in the honeycomb lattice [31]. The valence bands also exhibit Dirac cone features, both at the symmetry points (e.g., Γ and K) and along the symmetry lines. These Dirac-cone band structures are expected to contribute to the nontrivial band topology with finite Chern numbers when SOC is introduced.

We employed the WANNIER90 package [32], to calculate the maximally localized Wannier functions (MLWFs), to in turn characterize the topology of each band, and constructed a tight-binding Hamiltonian to fit to the DFT band structures. From the tight-binding Hamiltonian, we calculated the Chern numbers (C_n) of each individual band by integrating their Berry curvatures [$\Omega_{n,z}(\mathbf{k})$] over the Brillouin zone (BZ). As a result, the conduction and valence bands with SOC in Fig. 1(d) are labeled with their calculated Chern numbers (C_n). All of the conduction and valence bands have nontrivial band topologies. Further, there are several bands with high Chern numbers.

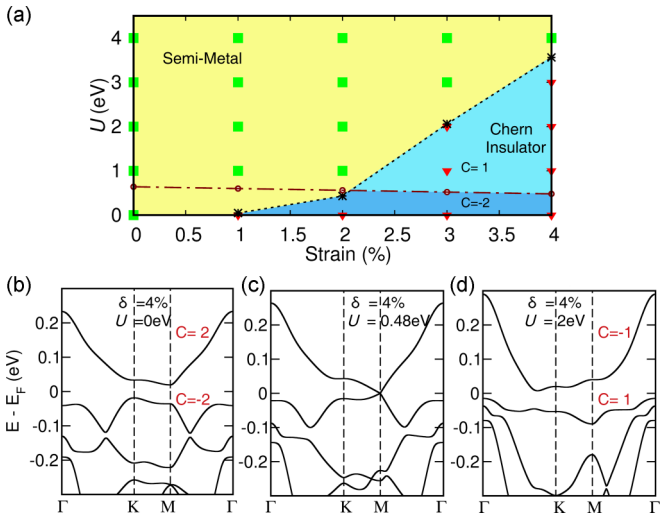

FIG. 2. Electronic structure and topological quantum phase transition (TQPT) of hole-doped single-layer CrI_3. (a) The TQPT diagram for the Hubbard U versus the epitaxial strain. (b) PBE+SOC band structure at 4% epitaxial strain with total Chern number $C = -2$. (c) The band structure with quantum critical point $U_{c1} = 0.48$ eV exhibiting gap closing at M. (d) The PBE+U+SOC band structure at $U > U_{c1}$ with total Chern number $C = 1$.

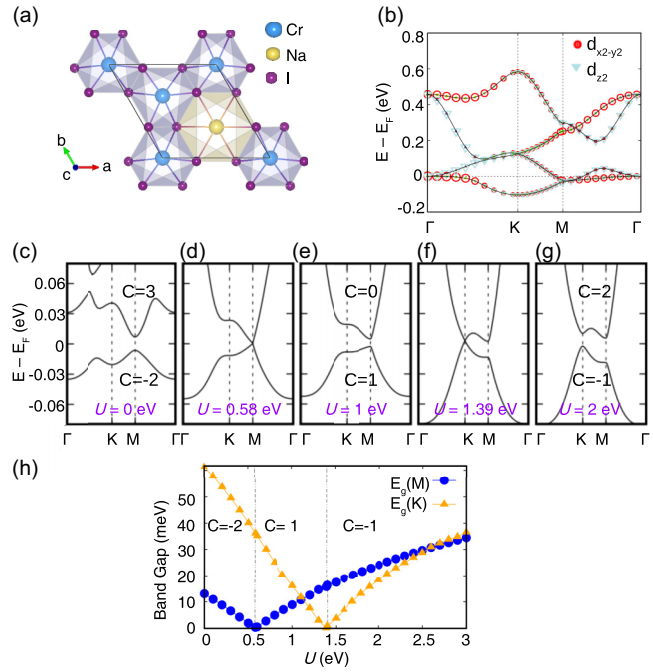

FIG. 3. The electronic structure of electron-doped single-layer CrI_3. (a) The crystal structure of Na doped CrI_3 in the ab plane. (b) Fatband projection of Cr d orbitals in local coordinates under the PBE approximation for Na doping. (c)–(g) The evolution of the HOB and LUB near the Fermi level with increasing Hubbard U under the PBE+U+SOC approximation. The gap closing occurs at two U values $U_{c1} = 0.58$ eV and $U_{c2} = 1.39$ eV. (h) The evolution of the band gap at the K and M points with the Hubbard U.

The presence of conduction and valence bands with nontrivial Chern numbers across the band gap in CrI_3 provides a unique opportunity to control its transport properties, as well as to drive electronic and topological phase transitions by charge doping. A recent experimental demonstration of the electrostatic gate control of the magnetism in both monolayer and bilayer CrI_3 [21,22] suggests that this 2D material is an ideal case for the study of tunable topological properties. Indeed, electrostatic doping has become an important practical method for driving electronic phase transitions [33], and to control the magnetic [34] and optical properties [35].

A. Hole-doped monolayer

We introduced a homogeneous background charge of $\Delta n_e = -1$ to simulate the electrostatic control of hole doping in monolayer CrI_3, and carried out self-consistent DFT calculations. The self-consistent band structure for the hole-doped ($\Delta n_e = -1$) monolayer CrI_3 was found to be close to that of the rigid-band shift of E_F, as shown in Fig. 1(d), maintaining its half-metallic FM state, where the Fermi level crosses two separate bands with a negative indirect gap. However, in the case of the Cr d electrons, the two bands that cross E_F in hole-doped CrI_3 are sensitive to both the lattice strain and the on-site Coulomb interactions. Figure 2(a) shows a relatively large band gap of ~38 meV for a tensile strain of 4%, but the band gap opening starts at a much smaller strain, of $\delta = 1\%$, even without turning on the on-site Coulomb interaction U, as illustrated in the strain-U phase diagram of Fig. 2(a).

At $U = 0$ eV, the tensile lattice strain of $\delta = 1\%$ drives the semimetal state into an insulating state with a Chern number $C = -2$. On the other hand, interesting band crossing behavior occurs when we increase U. As demonstrated in Figs. 2(b)–2(d), the conduction and valence bands of hole-doped CrI_3 with $\delta = 4\%$ strain undergoes a TQPT at $U_c = 0.48$ eV, where the Chern number changes from $C = -2$ to $C = 1$. Since this TQPT is not restricted to a particular value of the strain, we explored the whole range of possible strains and U parameters. The results are summarized in Fig. 2(a). The phase diagram is divided into three regions: semimetal, CI with $C = -2$, and another CI with $C = 1$. As the tensile strain increases, the insulating region becomes larger, indicating that the band gap is enhanced by strain. We noted that the TQPT from $C = -2$ to $C = 1$ occurs even in the semimetal region when the indirect gap is negative. This implies that the change of U is responsible for the TQPT, i.e., the band inversion at the M point, while the semimetal-to-insulator transition is driven by the lattice strain [36].

B. Electron-doped monolayer

Electron doping can be achieved in several ways in addition to via electrostatic gate control, such as by intercalation or adatom deposition of alkaline atoms. Similar studies have been reported in previous works on thin films [37,38]. In this work, we present the results of using Na adatom doping to achieve one-electron doping per $(CrI_3)_2$ unit cell of monolayer CrI_3, as illustrated in Fig. 3(a). The Na adatom is in the hollow region of the CrI_3 cell, i.e., at the center of the honeycomb, which is energetically stable. The cohesive energy calculation and thermodynamic stability is given in support of stability of Na-doped monolayer [36]. Figure 3(b) shows the band

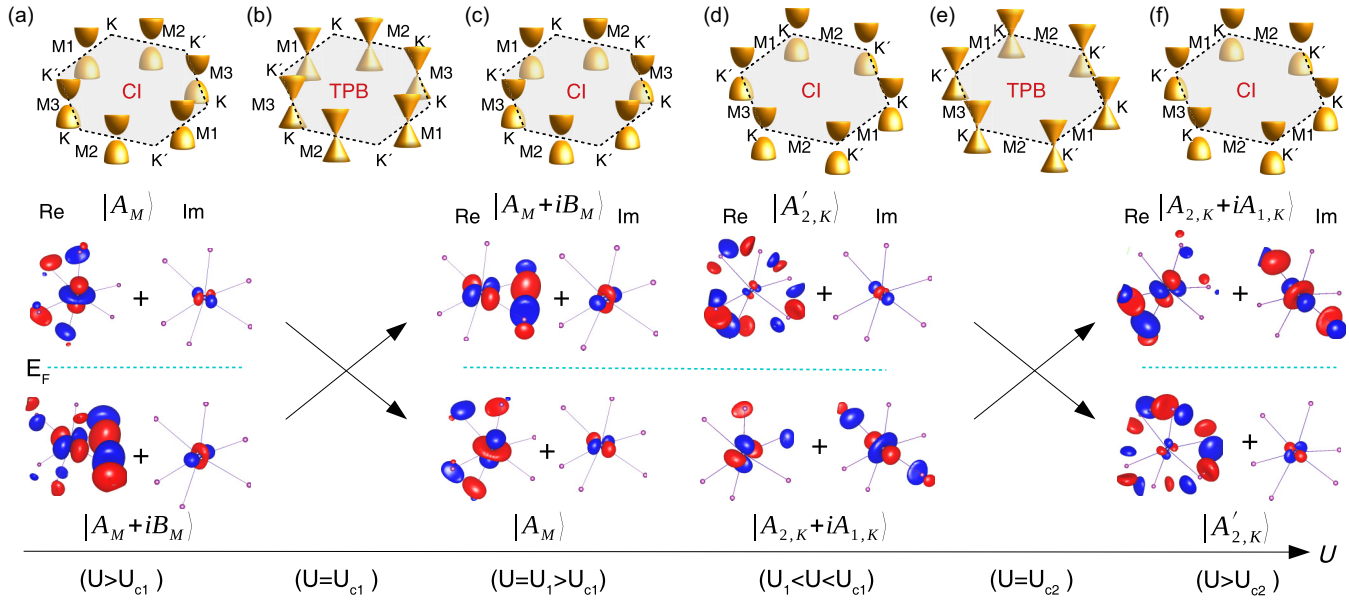

FIG. 4. The topological phase evolution with strong correlations due to band inversion in Na-doped CrI_3. (a)–(f). Schematic diagram of the evolution of the HOB and LUB of the Dirac crossings at all K and M points in the Brillouin zone (BZ) under the PBE+U+SOC approximation and the Real (Re) and imaginary (Im) parts of the corresponding MOs symmetry of the HOB and LUB are shown. The Fermi level (E_F) is indicated by the dashed cyan colored line between the HOMO and LUMO.

structure of the Na-doped CrI_3 monolayer without SOC for $U = 0$ eV. The Na doping almost causes a rigid-band shift of the Fermi level, but we did not observe any significant change in the band dispersion in comparison to pristine CrI_3, as shown in Fig. 1(c). We obtained a CI phase with $C = -2$ [see Fig. 3(c)] for $U = 0$ eV after including the SOC.

Similar to the hole-doped CrI_3 system, the electron-doped CrI_3 also underwent TQPTs as we introduced the on-site U to evaluate a realistic model for the Cr d electrons. The band structures shown in Figs. 3(c)–3(g) were calculated by the PBE+U+SOC method, with the on-site U for the Cr d orbitals varying from $U = 0$ eV to $U = 2$ eV. As U increases, the electron-doped CrI_3 changes from a CI with $C = -2$ to another CI with $C = 1$, then to another CI with $C = -1$. Two successive gap closings occur at the Fermi level as U increases, at the M point with $U_{c1} = 0.58$ eV and at the K point with $U_{c2} = 1.39$ eV. Figure 3(h) clearly demonstrates the topological phase transitions that occur alongside the band gap evolution at the K and M points when U increases. Considering that the optimal value of U for a Cr atom is ~3 eV, the practical SOC band gap of the electron-doped CrI_3 is predicted to be $\Delta_K \sim 19$ meV, which leads to a direct gap at the K point.

C. Topological quantum phase transition

We also evaluated the TQPT for the electron-doped case by investigating the symmetries of the highest occupied band (HOB) and the lowest unoccupied band (LUB) near E_F in terms of the irreducible representations (IRs) of the Little groups in the highly symmetric points of the BZ. The same analysis should be equally applicable to the hole-doped case.

Figure 4 illustrates a schematic drawing of the HOB and LUB across the entire BZ, along with the associated wave-function symmetry. The IRs at the M point with point group C_2 have $|A_M\rangle$ and $|B_M\rangle$, which are, respectively, even and odd with respect to the twofold rotation along the Γ-M line at $U < U_{c1}$. In the presence of FM ordering, there are partial mixtures of the opposite parity states in the imaginary parts of both the HOB and LUB states due to the SOC term. The wave functions go through an inversion [Fig. 4(c)] after passing through the topological phase boundary (TPB) [Fig. 4(b)] ($U = U_{c1}$). Consequently, the band inversions at the three M points in the BZ contribute to a total change in the Chern number of $\Delta C = 3$, so that the TQPT across $U = U_{c1}$ occurs from a CI with $C = -2$ to another CI with $C = 1$. A similar phenomenon occurs at the K point, where the point group symmetry is D_3. Thus, the relevant IRs at K are $|A_{2,K} + iA_{1,K}\rangle$ and $|A'_{2,K}\rangle$, which correspond to $|A_M\rangle$ and $|B_M\rangle$ at M, respectively. Again, crossing the TPB at $U = U_{c2}$, the HOB and LUB states touch at the K point [Fig. 4(e)] and cause the Chern number to change by $\Delta C = 2$. This change arises from the fact that there are two K points in the BZ, which causes the Chern number to change from $C = 1$ to $C = -1$ at $U = U_{c2}$.

D. Topological properties

Figure 5 summarizes the topological properties of Na-doped CrI_3. The calculated Berry curvatures, $\Omega_{n,z}(\mathbf{k})$, and the anomalous Hall conductivity σ_z for $U = 0$, 1, and 2 eV are plotted in Figs. 5(b) and 5(a). The total Chern number C is calculated by integrating the Berry curvature over the first BZ while tuning the Fermi level. The anomalous Hall conductivity, σ_z, in the unit of quantum conductance, e^2/h, is calculated as a function of the Fermi level. The steplike change of σ_z at E_F reflects the Chern numbers of $C = -2$ for $U = 0$ eV, $C = 1$ for $U = 1$ eV, and $C = -1$ for $U = 2$ eV. The sign change of the Chern number is also reflected in the Berry curvature plot. This anomalous Hall conductivity

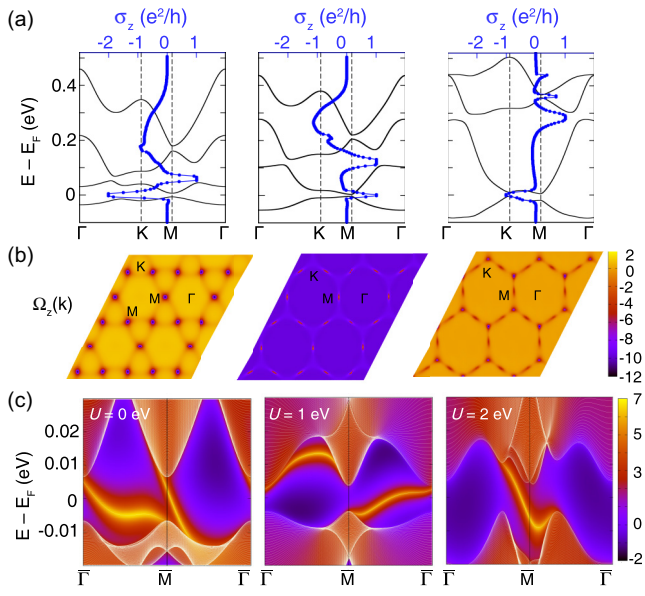

FIG. 5. Topological properties in Na-doped CrI_3. (a) The anomalous Hall conductivity σ_z as a function of the energy for $U = 0$ eV, 1 eV, and 2 eV. (b) The Berry curvature under the PBE+U+SOC model, at $U = 0$ eV, 1 eV, and 2 eV in the BZ. (c) The edge Green's function for the left edge of the slab under PBE+U+SOC at $U = 0$ eV, 1 eV, and 2 eV.

results also indicate that even only a fractional number of electron or hole doping would show large anomalous Hall conductivity.

The Berry curvature at $U = 0$ eV [Fig. 5(b)] shows that the negative peaks are only at the M points in the BZ, which should lead to the total Chern number being $C = -3$ instead of -2. However, the PBE band structure in the electron-doped case includes two linear Dirac crossings at Γ and along the Γ-M line in the BZ. Simply including SOC under the PBE+SOC assumption induces two band inversions at the Γ and M points. By changing the intrinsic SOC for the I p orbital (which is the key factor affecting the SOC in this material) from $\lambda^{SO}_{I-p} = 0$ to $\lambda^{SO}_{I-p} = 1$, we observe a positive Berry peak around the Γ point at a smaller $\lambda^{SO}_{I-p} = 0.2$, where the gap $\Delta_{\mathrm{gap},\Gamma}$ at Γ is reasonably small. However, the peak spreads homogeneously over all of the BZ at $\lambda^{SO}_{I-p} = 1$ due to the wide gap ($\Delta_{\mathrm{gap},\Gamma}$) at the Γ point, while still contributing $\Delta C = 1$ to the total Chern number [36]. This additional background Berry curvature remains throughout the U regime.

We confirmed the change in the value and sign of the Chern number with increasing U by calculating the edge states using the edge Green's function with the surface-projected density of states [39]. Only the left edge of the slab is shown in Fig. 5(c) for $U = 0$, 1, and 2 eV. The winding of the edge state clearly shows that the sign of the Chern number is in agreement with the calculated Wilson loop for $U = 0$, 1, and 2 eV [36].

IV. SUMMARY

In summary, we have demonstrated that the recently synthesized monolayer CrI_3 exhibits nontrivial band topologies in both the valence and conduction bands. We achieved a CI state by charge doping, which is equivalent to the electrostatic gating in practice. Further, we observed a tunable magnetic topological insulator phase in electron- and hole-doped monolayer CrI_3 by controlling the on-site Coulomb interaction for Cr d electrons. The spin-momentum locking at the edges and control over the chirality of the edge states of the charge doped monolayer CrI_3 open up new possibilities for the electronic manipulation of spin in topological spintronic devices. In addition, the epitaxial strain was found to play a significant role in the study of the semimetal-to-CI transition in hole-doped monolayer CrI_3. Monolayer CrI_3 with charge doping, which should be practically realizable, was found to be as stable as the pristine monolayer CrI_3. Although no systematic study of the possible topological properties of monolayer CrI_3 has yet been reported, the physical properties of charge-doped monolayer CrI_3 will facilitate future studies on materials that potentially exhibit novel topological phenomena.

ACKNOWLEDGEMENT

We gratefully acknowledge Robert-Jan Slagger and Seungjin Kang for valuable discussions. This work is supported by Institute for Basic Science (IBS) in Korea (Grant No. IBS-R009-D1). J.Y. acknowledges the support by the National Research Foundation of Korea (NRF) (No. 2017R1A2B4007100) and the support and hospitality provided by the Max Planck Institute for the Physics of Complex systems during his visit to the institute.

[1] Y. Xue, B. Zhao, Y. Zhu, T. Zhou, J. Zhang, N. Li, H. Jiang, and Z. Yang, NPG Asia Mater. **10**, 467 (2018).
[2] Y.-J. Song, K.-H. Ahn, W. E. Pickett, and K.-W. Lee, Phys. Rev. B **94**, 125134 (2016).
[3] P. Zhou, C. Q. Sun, and L. Z. Sun, Nano Lett. **16**, 6325 (2016).
[4] D. J. Thouless, M. Kohmoto, M. P. Nightingale, and M. den Nijs, Phys. Rev. Lett. **49**, 405 (1982).
[5] F. D. M. Haldane, Phys. Rev. Lett. **61**, 2015 (1988).
[6] M. Z. Hasan and C. L. Kane, Rev. Mod. Phys. **82**, 3045 (2010).
[7] C.-Z. Chang, J. Zhang, X. Feng, J. Shen, Z. Zhang, M. Guo, K. Li, Y. Ou, P. Wei, L.-L. Wang, Z.-Q. Ji, Y. Feng, S. Ji, X. Chen, J. Jia, X. Dai, Z. Fang, S.-C. Zhang, K. He, Y. Wang, L. Lu, X.-C. Ma, and Q.-K. Xue, Science **340**, 167 (2013).
[8] C.-X. Liu, X.-L. Qi, X. Dai, Z. Fang, and S.-C. Zhang, Phys. Rev. Lett. **101**, 146802 (2008).
[9] R. Yu, W. Zhang, H.-J. Zhang, S.-C. Zhang, X. Dai, and Z. Fang, Science **329**, 61 (2010).
[10] K. Yasuda, M. Mogi, R. Yoshimi, A. Tsukazaki, K. S. Takahashi, M. Kawasaki, F. Kagawa, and Y. Tokura, Science **358**, 1311 (2017).
[11] K. v. Klitzing, G. Dorda, and M. Pepper, Phys. Rev. Lett. **45**, 494 (1980).

[12] C.-Z. Chang, W. Zhao, D. Y. Kim, H. Zhang, B. A. Assaf, D. Heiman, S.-C. hang, C. Liu, M. H. W. Chan, and J. S. Moodera, Nature Mater. **14**, 473 (2015).
[13] A. R. Mellnik, J. S. Lee, A. Richardella, J. L. Grab, P. J. Mintun, M. H. Fischer, A. Vaezi, A. Manchon, E.-A. Kim, N. Samarth, and D. C. Ralph, Nature (London) **511**, 449 (2014).
[14] K. Yasuda, A. Tsukazaki, R. Yoshimi, K. Kondou, K. S. Takahashi, Y. Otani, M. Kawasaki, and Y. Tokura, Phys. Rev. Lett. **119**, 137204 (2017).
[15] K. S. Novoselov, A. Mishchenko, A. Carvalho, and A. H. Castro Neto, Science **353**, aac9439 (2016).
[16] J. Liu, S. Y. Park, K. F. Garrity, and D. Vanderbilt, Phys. Rev. Lett. **117**, 257201 (2016).
[17] Q. Sun and N. Kioussis, Phys. Rev. B **97**, 094408 (2018).
[18] J. He, S. Ma, P. Lyu, and P. Nachtigall, J. Mater. Chem. C **4**, 2518 (2016).
[19] M. A. McGuire, H. Dixit, V. R. Cooper, and B. C. Sales, Chem. Mater. **27**, 612 (2015).
[20] A. Downs and C. Adams, in *The Chemistry of Chlorine, Bromine, Iodine and Astatine*, Pergamon Texts in Inorganic Chemistry, Vol. 7, edited by A. Downs and C. Adams (Pergamon, Oxford, 1973), pp. 1107–1594.
[21] B. Huang, G. Clark, D. R. Klein, D. MacNeill, E. Navarro-Moratalla, K. L. Seyler, N. Wilson, M. A. McGuire, D. H. Cobden, D. Xiao, W. Yao, P. Jarillo-Herrero, and X. Xu, Nature Nanotechnol. **13**, 544 (2018).
[22] S. Jiang, L. Li, Z. Wang, K. F. Mak, and J. Shan, Nature Nanotechnol. **13**, 549 (2018).
[23] J. P. Perdew, K. Burke, and M. Ernzerhof, Phys. Rev. Lett. **77**, 3865 (1996).
[24] G. Kresse and D. Joubert, Phys. Rev. B **59**, 1758 (1999).
[25] G. Kresse and J. Furthmüller, Phys. Rev. B **54**, 11169 (1996).
[26] T. Ozaki, Phys. Rev. B **67**, 155108 (2003).
[27] Y. Liu and C. Petrovic, Phys. Rev. B **97**, 014420 (2018).
[28] B. Huang, G. Clark, E. Navarro-Moratalla, D. R. Klein, R. Cheng, K. L. Seyler, D. Zhong, E. Schmidgall, M. A. McGuire, D. H. Cobden, W. Yao, D. Xiao, P. Jarillo-Herrero, and X. Xu, Nature (London) **546**, 270 (2017).
[29] J. L. Lado and J. Fernández-Rossier, 2D Mater. **4**, 035002 (2017).
[30] W.-B. Zhang, Q. Qu, P. Zhu, and C.-H. Lam, J. Mater. Chem. C **3**, 12457 (2015).
[31] Y. Sugita, T. Miyake, and Y. Motome, Phys. Rev. B **97**, 035125 (2018).
[32] A. A. Mostofi, J. R. Yates, Y.-S. Lee, I. Souza, D. Vanderbilt, and N. Marzari, Comput. Phys. Commun. **178**, 685 (2008).
[33] Y. Saito, T. Nojima, and Y. Iwasa, Nat. Rev. Mater. **2**, 16094 (2016).
[34] K. S. Novoselov, Rev. Mod. Phys. **83**, 837 (2011).
[35] Z. Sun, A. Martinez, and F. Wang, Nat. Photonics **10**, 227 (2016).
[36] See Supplemental Material at http://link.aps.org/supplemental/10.1103/PhysRevB.98.155148 for the origin of the semimetal-to-insulator transition in hole-doped monolayer CrI_3, the origin of the Chern number $C = -2$ in the electron-doped CrI_3, the change of the calculated Wilson loop with U, the thermodynamic stability and estimate of cohesive energy of Na-doped monolayer CrI_3 and pristine monolayer CrI_3, which includes Refs. [2,39–41].
[37] M. Zribi, M. Kanzari, and B. Rezig, Mater. Lett. **60**, 98 (2006).
[38] A. Chelouche, T. Touam, F. Boudjouan, D. Djouadi, R. Mahiou, A. Bouloufa, G. Chadeyron, and Z. Hadjoub, J. Mater. Sci.: Mater. Electron. **28**, 1546 (2017).
[39] Q. Wu, S. Zhang, H.-F. Song, M. Troyer, and A. A. Soluyanov, Comput. Phys. Commun. **224**, 405 (2018).
[40] A. O.-de-la Roza and V. Luaña, Comput. Phys. Commun. **182**, 1708 (2011).
[41] A. O.-de-la Roza, D. Abbasi-Pérez, and V. Luaña, Comput. Phys. Commun. **182**, 2232 (2011).